Role of active metals Cu, Co, and Ni on ceria towards CO_2 thermo-catalytic hydrogenation

Henrik Bali[1,+], Suresh Mutyala[1,+], Anastasiia Efremova[1], Shaohua Xie[2,+], Samantha Collier[2], Ábel Marietta[1], András Sápi[1,*], Fudong Liu[2], Ákos Kukovecz[1], Zoltán Kónya[1,3]

[1]*Department of Applied and Environmental Chemistry, Interdisciplinary Excellence Centre, University of Szeged, H-6720, Rerrich Bela ter 1, Szeged, Hungary*

[2]*Department of Civil, Environmental, and Construction Engineering, Catalysis Cluster for Renewable Energy and Chemical Transformations (REACT), NanoScience Technology Center (NSTC), University of Central Florida, Orlando, FL 32816, United States*

[3]*MTA-SZTE Reaction Kinetics and Surface Chemistry Research Group, University of Szeged, Rerrich Béla tér 1, Szeged 6720, Hungary*

Corresponding author: Email address: sapia@chem.u-szeged.hu (András Sápi)

Abstract

A series of CeO_2 supported Cu, Co, and Ni catalysts have been synthesized by the wet-impregnation method for CO_2 thermo-catalytic hydrogenation from 200 – 400 °C in the fixed bed reactor. All catalysts were characterized by XRD, N_2-isotherms, and H_2 temperature-programmed reduction. XRD results have suggested that the incorporated Cu, Co, and Ni have uniformly distributed on the CeO_2 surface, N_2-isotherm analysis confirmed that the pores of CeO_2 were blocked by incorporated metals and H_2-TPR indicated strong interaction between active metal and CeO_2. The CO_2 consumption rate and product selectivity depend on the type of active metal on CeO_2 and reaction temperature. The order of CO_2 consumption rate for 5wt% catalysts was $5Ni/CeO_2 > 5Co/CeO_2 > 5Cu/CeO_2$ at 400 °C. The high CO_2 consumption rate for $5Ni/CeO_2$ was attributed to the presence of more number of active metallic Ni during the reaction which dissociated H_2 molecule to H-atoms. The formed H-atoms reacted with active CO_2 molecule and formed CH_4 with 100% selectivity.

Keywords: Metals (Cu, Co, and Ni); CeO_2; Carbon dioxide; Hydrogenation; Fixed bed reactor

1. Introduction

Carbon dioxide is one of the environmental pollutant gases which is liberated by the use of fossil fuels, high growth of petrochemical and automobile industries. It causes global-warming in the atmosphere. The concentration of CO_2 in the atmosphere can be diminished by the capture and utilization or storage (CCUS) [1]. Among these methods, CO_2 utilization is the most important one. In this method, CO_2 is converted into chemicals and fuels such as CO, hydrocarbons, and

alcohols using a solid catalyst [2-4]. The products are used as fuel and important feedstock in the chemical industry.

$CO_2 + H_2 \rightarrow CO + H_2O$	$\Delta H_{298\,K}$ = +41 kJ/mol	RWGS reaction
$CO_2 + 4H_2 \rightarrow CH_4 + 2H_2O$	$\Delta H_{298\,K}$ = -165 kJ/mol	Sabatier reaction
$CO_2 + H_2 \rightarrow CH_3OH + H_2O$	$\Delta H_{298\,K}$ = - 49.5 kJ/mol	Methanol synthesis

Active metal-supported catalysts such as Pt [5], Pd [6], Ru [7], Rh [8], Co [9], and Ni [10] have been used for the study of CO_2 catalytic hydrogenation. In these metals, Ru, Rh, Pt, and Pd supported catalyst have shown high CO_2 utilization. However, these metals are very expensive. Therefore, non-noble metals such as Cu, Co, and Ni supported catalysts are useful for CO_2 hydrogenation. The selectivity of CO or CH_4 depends on the type of catalyst, support, and reaction conditions. The CO_2 catalytic hydrogenation at high-temperature results in coke formation on the surface of the catalyst which deactivates the active metal. It can be overcome by the use of selective support. Metal oxides like Al_2O_3 [11], ZrO_2 [12], SiO_2 [13], carbon materials [14, 15], CeO_2 [16], TiO_2 [17], and MnO_2 [18] were used as supports to deposit the active metals for the study of CO_2 catalytic hydrogenation.

Among these supports, CeO_2 has high oxygen storage capacity and redox property which enhances the catalytic activity [19]. T.A. Le et al have studied CO and CO_2 hydrogenation over Ni supported on different supports such as SiO_2, TiO_2, γ-Al_2O_3, ZrO_2, and CeO_2 [20]. In this article, we have chosen CeO_2 as the support and incorporated different non-noble metals like Cu, Co, and Ni to find out CO_2 consumption rate in CO_2 thermo-catalytic hydrogenation and selectivity of the products CO or CH_4 in the temperature range from 225 – 400 °C in the fixed bed reactor under atmospheric pressure.

2. Experimental

2.1 Chemicals

Analytical grade chemicals such as copper (II) nitrate trihydrate ($Cu(NO_3)_2.3H_2O$), cobalt (II) nitrate hexahydrate ($Co(NO_3)_2.6H_2O$), nickel (II) nitrate hexahydrate ($Ni(NO_3)_2.6H_2O$), and ammonia solution (NH_3, 25wt%) were purchased from the M/s. Across organics, Germany. The commercial ceria (CeO_2) was purchased from the M/s. Rhodia Company, France. All chemicals were used without purification. Ultra-high pure gases such as carbon dioxide, hydrogen, nitrogen, helium, and 10% (vol.) H_2/Ar was purchased from the M/s. Messer Company, Hungary.

2.2 Synthesis of CeO_2 supported Cu, Co, and Ni catalysts

The CeO_2 supported Cu, Co, and Ni catalysts were synthesized by the incipient wet impregnation method. Briefly, a desired quantity of copper (II) nitrate trihydrate solution was added dropwise to CeO_2 support then dried at 120 °C for 12 h followed by calcination at 550 °C for 2 h with a heating rate of 5 °C/min in static air. The calcined sample was denoted as xCu/CeO_2. (Where x was 1, 5, and 10 wt %). Similarly, Co and Ni supported on CeO_2 were also synthesized

by the same method as that of Cu/CeO_2 and denoted as yCo/CeO_2 and zNi/CeO_2. Where y and z represent wt% of Co and Ni. (Where y and z = 1, 5, and 10 wt %).

2.3 Characterization

The Rigaku Miniflex-II X-ray diffractometer was used to record the X-ray diffractions of CeO_2 supported catalysts using Ni filtered Cu K_α radiation having tube voltage 30 KV and current 15 mA. The Quantachrome NOVA 3000e gas adsorption analyzer was used to measure N_2 adsorption-desorption isotherms at 77 K. Before N_2 measurement, the sample was degasified at 300 °C for 2 h under vacuum. The specific surface area was calculated by the Brunauer-Emmett-Teller (BET) method. The pore size was calculated from desorption isotherm by the Barret-Joyner-Halenda (BJH) method. Total pore volume was calculated at a relative pressure of $P/P_0 = 0.99$. The hydrogen temperature-programmed reduction (H_2-TPR) was carried out using the Quantachrome Autosorb-iQ instrument. About, 30 mg of sample was loaded in a U-type micro-reactor and heated at 300 °C for 1 h in an inert gas to remove moisture then cooled to room temperature. After cooling to room temperature, the sample was exposed to 10% H_2 balanced Ar (v/v) with a flow rate of 50 mL/min and heated to 850 °C with a heating rate of 10 °C/min. The effluent H_2 concentration was monitored using a thermal conductivity detector (TCD).

2.4 Catalytic hydrogenation of CO_2

The CO_2 thermo-catalytic hydrogenation has been studied in the fixed bed reactor having an 8 mm ID and 200 mm length at atmospheric pressure. The reactor dead volume was filled with quartz beads. The gas reactants and temperature of the reaction were monitored using the mass-flow controller and PID controller. The gas line out of the reactor was kept at 150 °C to avoid the condensation. About, 0.15 g of the catalyst was loaded at the center of the reactor, CO_2/H_2 (1:4 vol. %) flow rate 50 mL/min, and temperature 225 – 400 °C were maintained. Before studying the reaction, Cu and Ni catalysts were reduced with hydrogen at 400 °C for 2h and Co catalysts were reduced at 500 °C for 2h. The composition of the gas came out from the reactor was analyzed by online-gas chromatography Agilent 6890N having a thermal-conductivity detector and flame-ionization detector. CO_2 conversion and consumption rate, CH_4, and CO selectivity were calculated using the formulas presented in the article [21].

3. Results and discussion

3.1 Structural characterizations

Fig. 1 shows the XRD patterns of CeO_2 supported Cu, Co, and Ni catalysts. CeO_2 has shown major diffraction peaks at $2\theta = 28.4°$, 32.9°, 47.4°, and 56.2° that correspond to the planes (111), (200), (220), and (311) (JCPDS card no. 81-0792) (Fig. 1a) [22]. In Cu, Co and Ni supported on CeO_2, the diffraction peaks of CuO, Co_3O_4, and NiO have not appeared which indicated that incorporated metal oxides were highly distributed on the surface of CeO_2 or not in the detection limit of XRD (Fig. 1a-c). Xiaoxia et al have reported that there was no appearance of diffraction peaks of incorporated metal oxide on CeO_2 in low wt% of metal oxide [23].

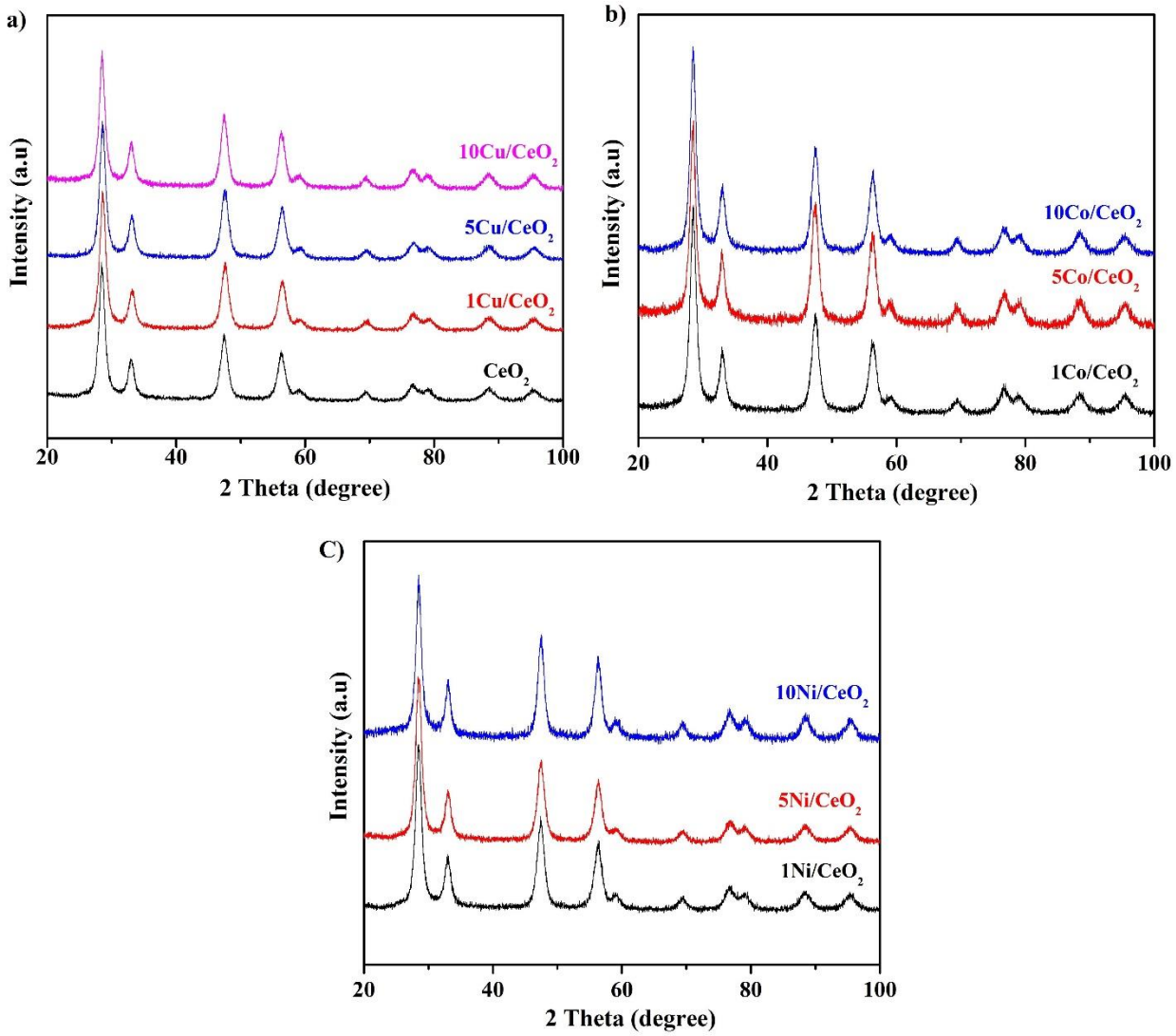

Fig. 1 XRD of CeO_2 supported Cu, Co, and Ni catalysts

The porosity of supported catalysts has been found by the N_2 adsorption-desorption isotherms at -196 °C. Fig. 2 shows the N_2 isotherms of CeO_2 supported Cu, Co, and Ni catalysts. The textural properties were presented in Table 1. Bare CeO_2 has shown a hysteresis loop in the relative pressure range $(P/P_0) = 0.4 – 1$ (Fig. 2a). The commercial CeO_2 shows type-IV adsorption-desorption isotherm with an H_2-hysteresis loop which indicates the presence of mesopores [24]. The specific surface area, pore size, and pore volume of commercial CeO_2 were 139.5 m^2/g, 8.95 nm, and 0.28 cm^3/g. The CeO_2 supported Cu, Co, and Ni catalysts have also shown an N_2-isotherm curve similar to bare CeO_2 (Fig. 2a-c). However, the quantity of N_2 adsorption capacity was decreased compared with bare CeO_2. It was due to the blockage of pores of CeO_2 by the incorporated metal oxide. Hence, the physical property values of the catalyst have been changed. For Cu supported on CeO_2 catalysts, the surface area, pore size, and pore volume decreased to 122.1 m^2/g, 8.4 nm, and 0.25 cm^3/gy. Co supported on CeO_2 catalysts have shown a decrease in

surface area, pore size, and pore volume to 121.9 m^2/g, 8.1 nm, and 0.24 cm^3/g. Similarly, Ni catalysts have also shown a decrease in textural property values.

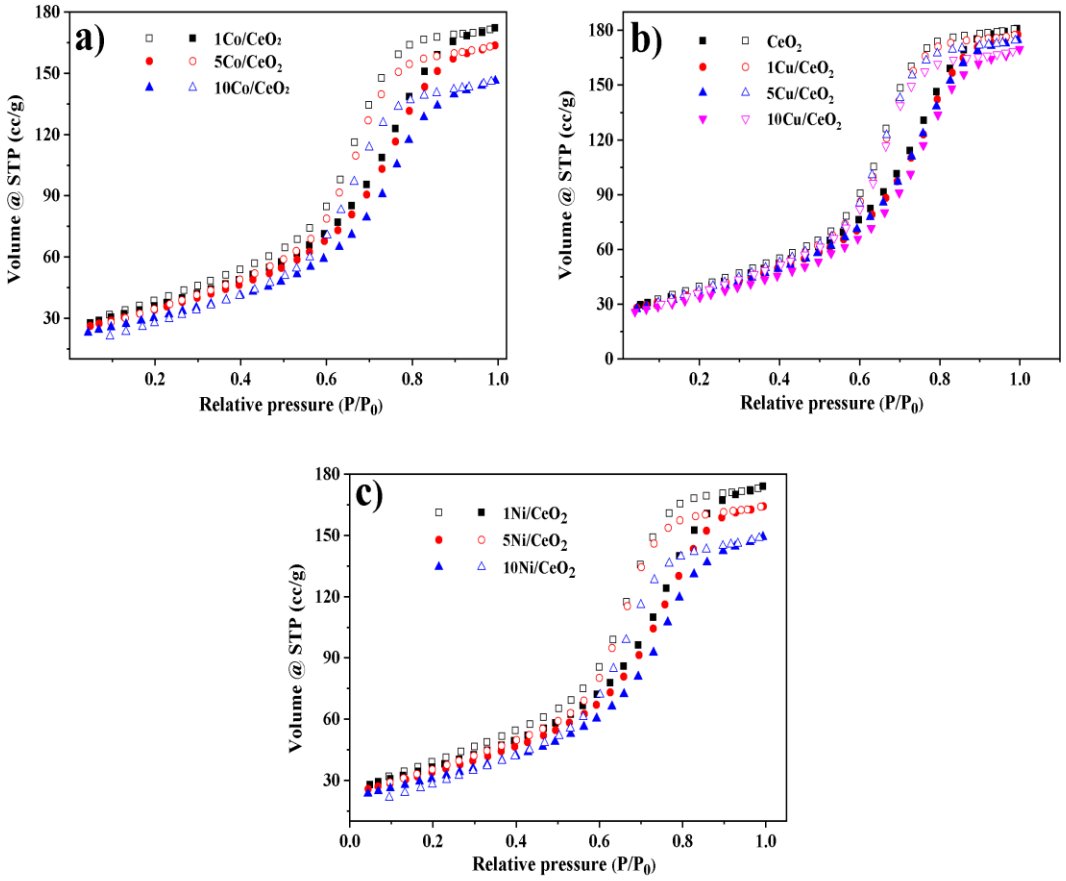

Fig. 2 N_2 adsorption-desorption isotherms of CeO_2 supported Cu, Co, and Ni catalysts

Table 1 Textural properties of bulk CeO_2 and CeO_2 supported Cu, Co, and Ni catalysts

Sample	Surface area (m^2/g)	Average pore size (nm)	Total pore volume (cm^3/g)
CeO_2	140	8.95	0.28
$1Cu/CeO_2$	133	8.17	0.27
$5Cu/CeO_2$	131	8.12	0.26
$10Cu/CeO_2$	122	8.4	0.25
$1Co/CeO_2$	132	7.9	0.26
$5Co/CeO_2$	130	8.0	0.25
$10Co/CeO_2$	121	8.1	0.24
$1Ni/CeO_2$	133	8.0	0.27
$5Ni/CeO_2$	129	8.1	0.26
$10Ni/CeO_2$	124	8.3	0.25

Fig. 3 shows the H_2 temperature-programmed reduction of CeO_2 supported Cu, Co, and Ni catalysts. Bare CeO_2 has shown reducible peaks at 300 °C, 372 °C, 486 °C and 786 °C which correspond to the reducibility of surface and lattice oxygen of CeO_2 [25]. In CeO_2 supported Cu catalysts, 2 major reducible peaks have appeared below 200 °C. For $1Cu/CeO_2$ catalyst, 2 reducible peaks have appeared at 156 °C and 174 °C which was related to the reducibility of copper species (CuO) on the surface on ceria and within the lattice of ceria (Cu-O-Ce). With an increase in copper content on ceria, the reducibility of these copper species icreased. Because of the high content of Cu on the surface and lattice of CeO_2 (Fig. 3a) [26].

With an increase in Co loading, the reduction peaks of surface Ce^{+4} shifted to a lower temperature. The reduction peaks at 220 °C and 265 °C for $5Co/CeO_2$, 197 °C and 234 °C for $10Co/CeO_2$ have represented the stepwise reduction of Co_3O_4 on the CeO_2 support [27]. Similarly, in CeO_2 supported Ni catalysts the reducible peaks of CeO_2 decreased to lower temperature compared to bare CeO_2 with an increase of Ni loading. The reducible peaks at 197 °C, around 250 °C, and 350 °C represent adsorbed and surface oxygen species of Ce^{+4} in nickel supported CeO_2 catalysts. The reducible peak at 300 °C for $5Ni/CeO_2$ and 306 °C for $10Ni/CeO_2$ showed NiO reducible peak. However, bulk Ce^{+4} reduction shifted to higher temperatures with an increase of Ni loading because of the strong interaction between Ni and CeO_2 (Fig. 3c) [28].

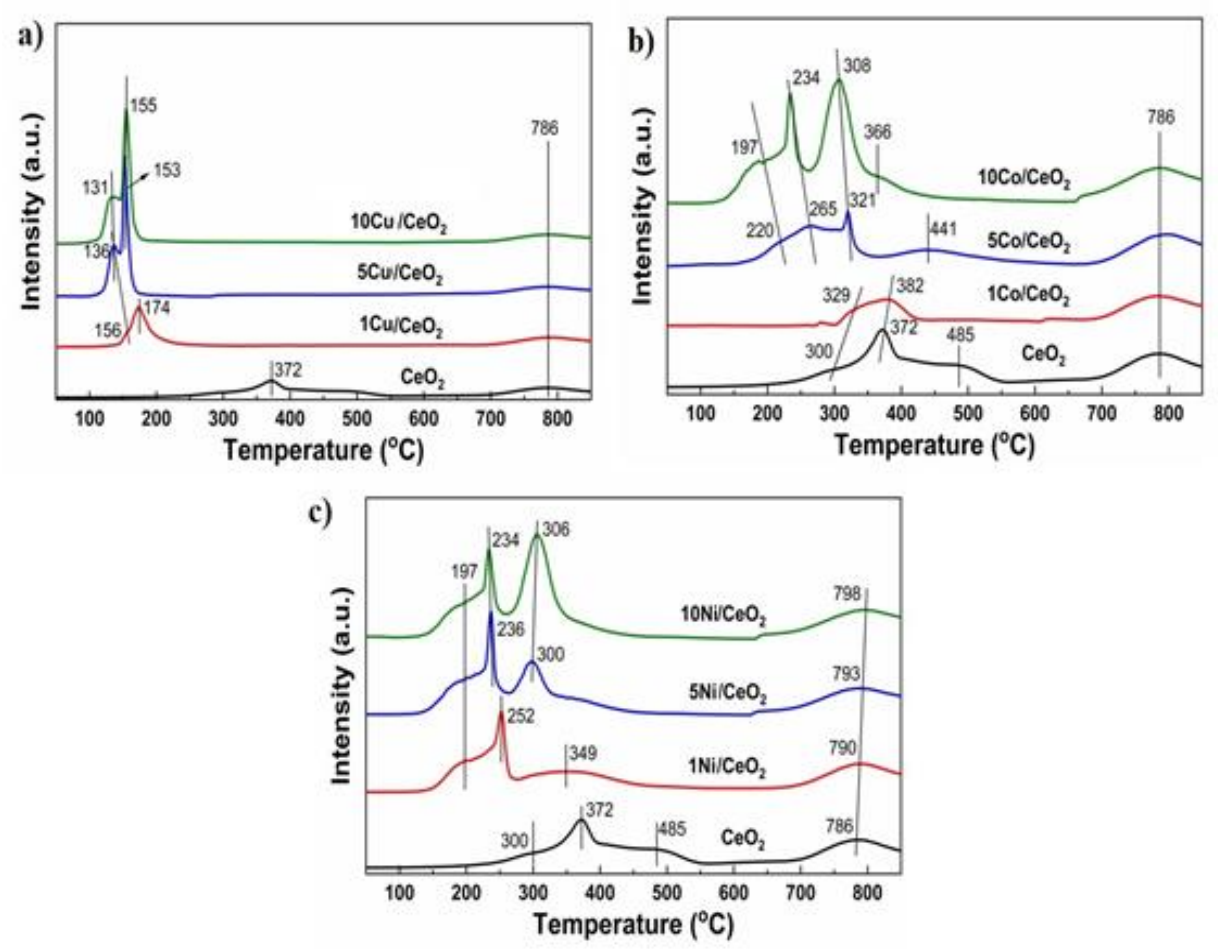

Fig. 3 H_2 temperature-programmed reduction of CeO_2 supported Cu, Co, and Ni catalysts

3.2 CO_2 catalytic hydrogenation

3.2.1 CeO_2 supported Cu catalysts

Fig. 4 shows the CO_2 catalytic hydrogenation of ceria supported Cu catalysts. The $10Cu/CeO_2$ catalyst has shown high CO_2 consumption rate at each reaction temperature because of high dispersion and more number of active Cu sites on the surface of CeO_2 compared to 1 wt% and 5 wt% of Cu on CeO_2 (Fig. 4a). The highest CO_2 consumption rate 9871 nmol/g/s was obtained for $10Cu/CeO_2$ catalyst at 400 °C. Moreover, CO selectivity was 100% for all Cu catalysts (Fig. 4b).

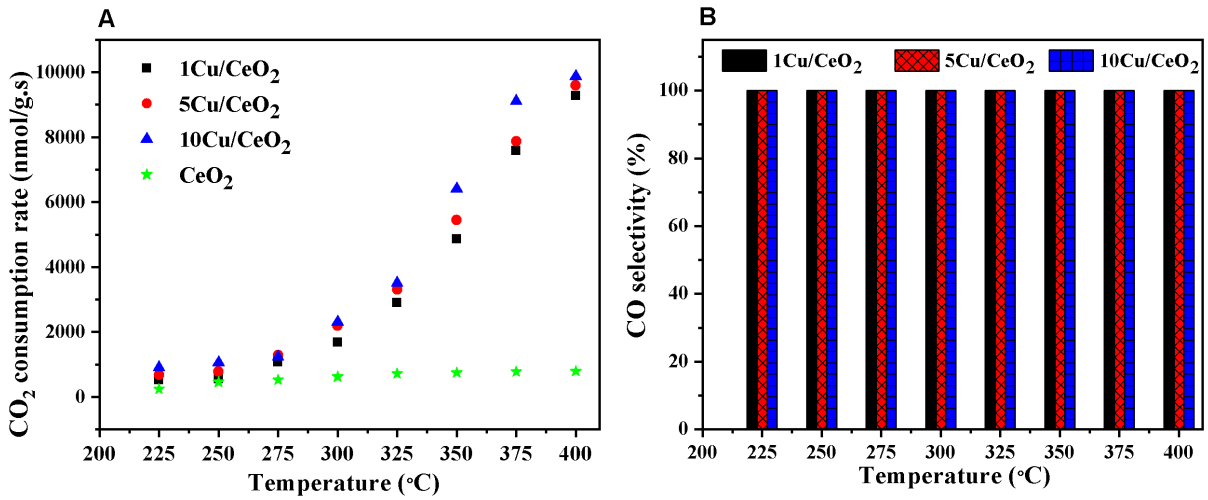

Fig. 4 a) CO_2 consumption rate and **b**) CO selectivity over CeO_2 supported Cu catalysts at different temperatures. Standard reaction conditions are defined as T = 225- 400 °C, P = Atmospheric, CO_2/H_2 = (1:4 V%), flow rate = 50 mL/min.

3.2.2 CeO_2 supported Co catalysts

CO_2 catalytic hydrogenation of Co/CeO_2 catalysts was shown in Fig. 5. The CO_2 consumption rate increased with an increase in temperature and formed products CO and CH_4. The obtained products have represented that CO_2 catalytic hydrogenation on Co/CeO_2 catalyst was proceeded in the following ways (Eqs. 1 and 2). First, CO_2 was converted into CO via reverse water gas shift reaction. The formed CO reacted with hydrogen and produced CH_4 [29].

$$CO_2 + H_2 \leftrightarrow CO + H_2O \quad (1)$$

Reverse water gas-shift reaction

$$CO + 3H_2 \rightarrow CH_4 + H_2O \quad (2)$$

The high content of cobalt on ceria, $10Co/CeO_2$ has shown a high CO_2 consumption rate compared to $1Co/CeO_2$ and $5Co/CeO_2$ throughout the temperature because higher number of CO_2 molecules were activated during the reaction (Fig. 5a). The highest CO_2 consumption rate was 9716 nmol/g.s for $1Co/CeO_2$, 14871 nmol/g.s for $5Co/CeO_2$ and 15853 nmol/g.s for $10Co/CeO_2$ at 400 °C. $1Co/CeO_2$ catalyst has shown 94.5% CO selectivity whereas ~ 81% CH_4 selectivity was obtained for $5Co/CeO_2$ and $10Co/CeO_2$ catalysts. It was represented that the high content of cobalt (5 and 10 wt%) on CeO_2 has gained a high CO_2 consumption rate and high CH_4 selectivity (Fig. 5b). In the time of stream study at 400 °C (Fig. 5c and d), $1Co/CeO_2$ has displayed a slight decrease in the CO_2 consumption rate and selectivity. However, $5Co/CeO_2$ and $10Co/CeO_2$ have shown a higher decrease in CO_2 consumption rate in long-duration by the formation of coke on the surface of the catalyst and a mild change in CO and CH_4 selectivity.

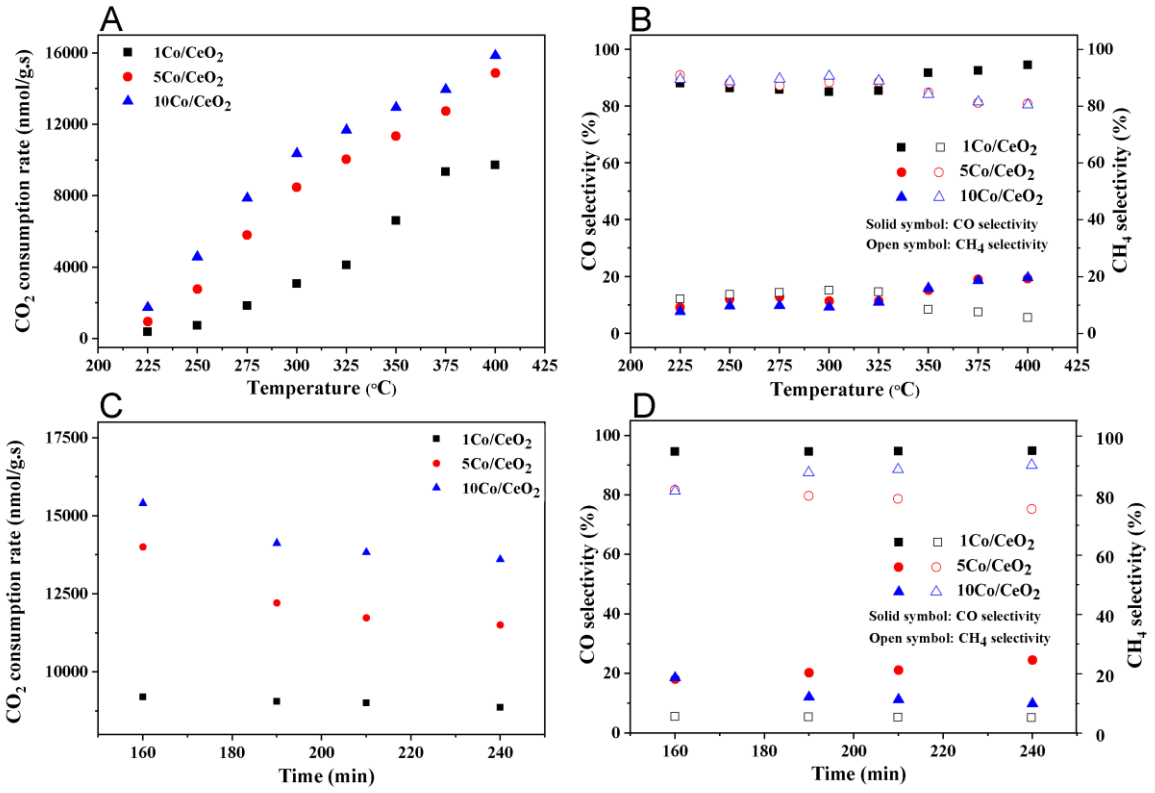

Fig. 5 a) CO_2 consumption rate **b**) CO and CH_4 selevtivity values for a H_2/CO_2 (4:1 vol. %) mixture in the range of 225 – 400 °C at atmospheric pressure. **c**,**d**) Time on stream at 400 °C over CeO_2 supported Co catalysts

3.2.3 CeO_2 supported Ni catalysts

CeO_2 supported Ni catalysts were also used for the catalytic hydrogenation of CO_2 and the results were presented in Fig. 6. The highest CO_2 consumption rate for each catalyst was shown in table 4. Among the synthesized Ni/CeO_2 catalysts, $5Ni/CeO_2$ has obtained a high CO_2 consumption rate of 32666 nmol/g.s with 100% CH_4 selectivity at 400 °C compared to that of $1Ni/CeO_2$ and $10Ni/CeO_2$ catalysts. The order of CO_2 consumption rate at 350 °C was $5Ni/CeO_2$ > $10Ni/CeO_2$ > $1Ni/CeO_2$ (Fig. 6a). Moreover, the selectivity of CH_4 on Ni/CeO_2 catalysts was > 97% (Fig. 6b). $10Ni/CeO_2$ has also reported a high CO_2 consumption rate up to 300 °C compared to the other two catalysts because of more accessible Ni metallic sites which were confirmed by H_2-TPR analysis (Fig. 3c). In supported Ni catalysts, the metallic Ni dissociates the H_2-molecule into H-atoms on the surface of the catalyst then the dissociated H-atoms are moved to active CO_2 molecule which is adsorbed on the support to form CH_4 [30].

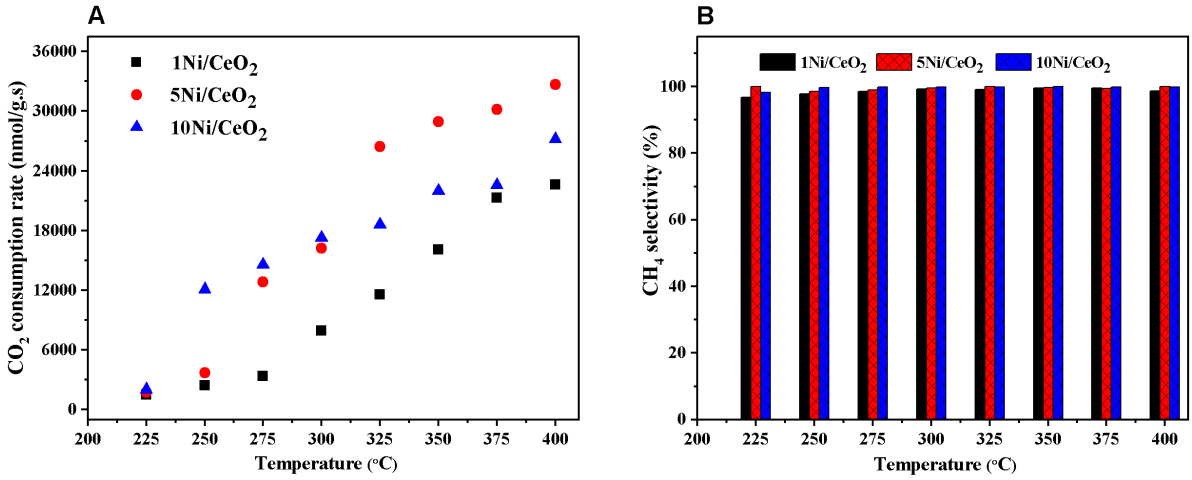

Fig. 6 a) CO_2 consumption rate and **b**) CH_4 selectivity over CeO_2 supported Ni catalysts at different temperatures. Standard reaction conditions are defined as T = 225- 400 °C, P = Atmospheric, CO_2/H_2 = (1:4 vol. %), flow rate = 50 mL/min.

3.2.4 Comparison of CO_2 consumption rates

For the comparison study, the CO_2 consumption rates of $5Cu/CeO_2$, $5Co/CeO_2$, and $5Ni/CeO_2$ catalysts at 400 °C were presented in Fig. 7. At all temperatures, $5Ni/CeO_2$ has obtained the highest CO_2 consumption rate compared with other catalysts. The order of CO_2 consumption rate was $5Ni/CeO_2 > 5Co/CeO_2 > 5Cu/CeO_2$. The metallic Ni was more active towards dissociation of H_2 molecule to H-atoms which reacted with more active CO_2 molecules. Hence, it showed a high CO_2 consumption rate compared with Cu and Co supported on CeO_2. The CO_2 catalytic hydrogenation of CeO_2 supported Cu, Co, and Ni catalysts have been compared with previously reported catalysts (Table 2). The CeO_2 supported non-noble metal (Cu, Co, and Ni) catalysts have shown high CO_2 consumption rate with high CO or CH_4 selectivity compared to some of the Co/KIT-6 [31], Fe/Al_2O_3 [32], Ni/TiO_2 [33] and Pt/MnO_2 [21] catalysts. Hence, CeO_2 supported catalysts are prominent for the study of CO_2 catalytic hydrogenation.

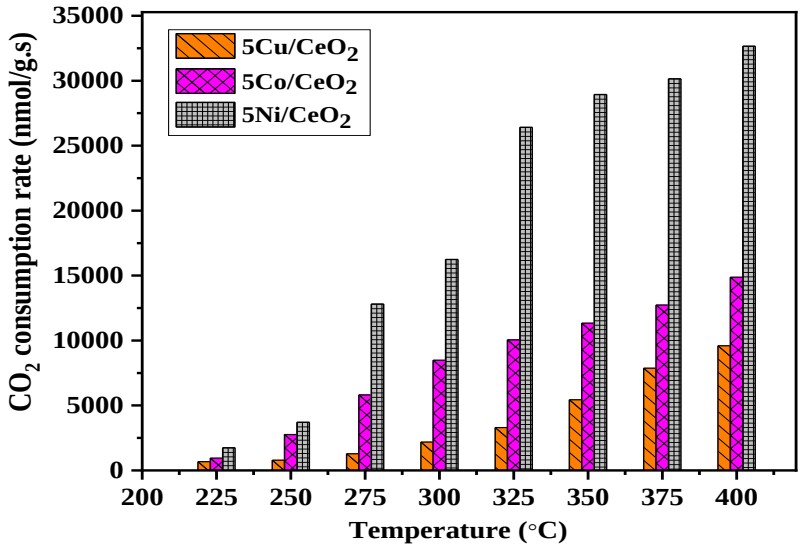

Fig. 7 CO_2 consumption rate of $5Cu/CeO_2$, $5Co/CeO_2$, and $5Ni/CeO_2$ catalysts

Table 2 Comparison of CO_2 conversion and consumption rate, CO and CH_4 selectivity of CeO_2 supported Cu, Co, and Ni catalysts with reported one

Catalyst	F_{CO_2} [a] (mL/s)	T [b] (°C)	X_{CO_2} [c] (%)	R_{CO_2} [d] (nmol/g/s)	S_{CO} [e] (%)	S_{CH_4} [f] (%)	Ref.
0.5wt% Pt/MnO_2	0.166	375 °C	25.3	12541	100	-	[21]
20wt% Co/KIT-6	0.061	280 °C	49	13335	-	100	[31]
15wt% Fe/Al_2O_3	0.166	500 °C	36	10707	90	10	[32]
15wt% Ni/TiO_2	0.133	260 °C	96	5716	-	100	[33]
15wt% Ni/Al_2O_3	0.333	325 °C	79	95178	-	98	[34]
$Ce_{1.1}Cu_1$ composite	0.083	400 °C	32.5	24166	100	-	[35]
5wt%Cu/CeO_2	0.166	400 °C	27.1	9594	100	-	Present work
5wt%Co/CeO_2	0.166	400 °C	58	14871	19	81	Present work
5wt%Ni/CeO_2	0.166	400 °C	80	32666	-	100	Present work

[a] F_{CO_2}: CO_2 flow rate (mL/s), [b] Temperature, [c] X_{CO_2}: CO_2 conversion, [d] R_{CO_2}:CO_2 consumption rate (nmol/g.s), [e] S_{CO}: CO selectivity, [f] S_{CH_4}: CH_4 selectivity.

4. Conclusion

In this work, we have reported the CO_2 consumption rate of CeO_2 supported Cu, Co, and Ni catalysts in CO_2 thermo-catalytic hydrogenation. The characterization results have confirmed the existence of active metals and strong interaction with CeO_2. The Ni supported catalysts have shown a high CO_2 consumption rate compared with Co/CeO_2 and Cu/CeO_2 catalysts. The selectivity of CH_4 was higher for Co and Ni supported on CeO_2 whereas CO selectivity was higher for Cu supported on CeO_2. Hence, the type of active metal and nature of support has influenced the CO_2 consumption rate and selectivity of the product.

Acknowledgment

This work was supported by the Startup Fund from the University of Central Florida (UCF). S. X. thanks the support from the Preeminent Postdoctoral Program (P3) at UCF. AS gratefully acknowledges the support of the Bolyai Janos Research Fellowship of the Hungarian Academy of Science and the "UNKP-20-5-SZTE-663" New National Excellence Program of the Ministry for Innovation and Technology from the source of the National Research, Development and Innovation Fund. The financial support of the Hungarian National Research, Development and Innovation Office through the GINOP-2.3.2-15-2016-00013 project "Intelligent materials based on functional surfaces - from syntheses to applications" and the Ministry of Human Capacities through the EFOP-3.6.1-16-2016-00014 project and the 20391-3/2018/FEKUSTRAT are acknowledged.

Author Information

[+]These authors contributed equally

Corresponding author: Email address: sapia@chem.u-szeged.hu (András Sápi)

References

[1] M. Aresta, A. Dibenedetto, A. Angelini (2014) Catalysis for the Valorization of Exhaust Carbon: from CO_2 to Chemicals, Materials, and Fuels. Technological Use of CO_2. Chem Rev. https://doi.org/10.1021/cr4002758

[2] E.V. Kondratenko, G. Mul, J. Baltrusaitis, G.O. Larrazábal, J. Pérez-Ramírez (2013) Status and perspectives of CO_2 conversion into fuels and chemicals by catalytic, photocatalytic and electrocatalytic processes. Energy Environ. Sci. https://doi.org/10.1039/C3EE41272E

[3] J.A. Rodriguez, J. Evans, L. Feria, A.B. Vidal, P. Liu, K. Nakamura, F. Illas (2013) CO_2 hydrogenation on Au/TiC, Cu/TiC, and Ni/TiC catalysts: Production of CO, methanol, and methane. J. Catal.
https://doi.org/10.1016/j.jcat.2013.07.023

[4] A. Modak, P. Bhanja, S. Dutta, B. Chowdhury, A. Bhaumik (2020) Catalytic reduction of CO_2 into fuels and fine chemicals. Green Chem.
https://doi.org/10.1039/D0GC01092H

[5] H. Choi, S. Oh, J.Y. Park (2020) High methane selective Pt cluster catalyst supported on Ga_2O_3 for CO_2 hydrogenation. Catal. Today.
https://doi.org/10.1016/j.cattod.2019.11.005

[6] H. Bahruji, M. Bowker, G. Hutchings, N. Dimitratos, P. Wells, E. Gibson, W. Jones, C. Brookes, D. Morgan, G. Lalev (2016) Pd/ZnO catalysts for direct CO_2 hydrogenation to methanol. J. Catal.
https://doi.org/10.1016/j.jcat.2016.03.017

[7] M.S. Maru, S. Ram, R.S. Shukla, N.-u.H. Khan (2018) Ruthenium-hydrotalcite (Ru-HT) as an effective heterogeneous catalyst for the selective hydrogenation of CO_2 to formic acid. J. Mol. Catal.
https://doi.org/10.1016/j.mcat.2017.12.005

[8] H. Kusama, K.K. Bando, K. Okabe, H. Arakawa (2000) Effect of metal loading on CO_2 hydrogenation reactivity over Rh/SiO_2 catalysts. Appl. Catal. A: Gen.
https://doi.org/10.1016/S0926-860X(99)00486-X

[9] K. Stangeland, D.Y. Kalai, Y. Ding, Z. Yu (2019) Mesoporous manganese-cobalt oxide spinel catalysts for CO_2 hydrogenation to methanol. J. CO2 Util.
https://doi.org/10.1016/j.jcou.2019.04.018

[10] G. Varvoutis, M. Lykaki, S. Stefa, E. Papista, S.A.C. Carabineiro, G.E. Marnellos, M. Konsolakis (2020) Remarkable efficiency of Ni supported on hydrothermally synthesized CeO_2 nanorods for low-temperature CO_2 hydrogenation to methane. Catal. Commun.
https://doi.org/10.1016/j.catcom.2020.106036

[11] T. Xie, J. Wang, F. Ding, A. Zhang, W. Li, X. Guo, C. Song (2017) CO_2 hydrogenation to hydrocarbons over alumina-supported iron catalyst: Effect of support pore size. J. CO2 Util.
https://doi.org/10.1016/j.jcou.2017.03.022

[12] Z. Zhang, L. Zhang, M.J. Hülsey, N. Yan (2019) Zirconia phase effect in Pd/ZrO_2 catalyzed CO_2 hydrogenation into formate. J. Mol. Catal. 457, 110461.
https://doi.org/10.1016/j.mcat.2019.110461

[13] W. Gac, W. Zawadzki, G. Słowik, A. Sienkiewicz, A. Kierys (2018) Nickel catalysts supported on silica microspheres for CO2 methanation. MICROPOR. MESOPOR. MAT.
https://doi.org/10.1016/j.micromeso.2018.06.022

[14] X.-L. Liang, X. Dong, G.-D. Lin, H.-B. Zhang (2009) Carbon nanotube-supported Pd–ZnO catalyst for hydrogenation of CO_2 to methanol. Appl. Catal. B: Env.
https://doi.org/10.1016/j.apcatb.2008.11.018

[15] S.-M. Hwang, C. Zhang, S.J. Han, H.-G. Park, Y.T. Kim, S. Yang, K.-W. Jun, S.K. Kim (2020) Mesoporous carbon as an effective support for Fe catalyst for CO_2 hydrogenation to liquid hydrocarbons. J. CO2 Util.
https://doi.org/10.1016/j.jcou.2019.11.025

[16] B. Ouyang, W. Tan, B. Liu (2017) Morphology effect of nanostructure ceria on the Cu/CeO_2 catalysts for synthesis of methanol from CO_2 hydrogenation. Catal. Commun.

[17] Z. Qin, X. Wang, L. Dong, T. Su, B. Li, Y. Zhou, Y. Jiang, X. Luo, H. Ji (2019) CO_2 methanation on Co/TiO_2 catalyst: Effects of Y on the support. Chemical Engineering Science.
https://doi.org/10.1016/j.ces.2019.115245

[18] J. Son, D. Song, K.R. Lee, J.-I. Han (2019) Electrochemical reduction of CO_2 on Ag/MnO_2 binary catalyst. J. Environ. Chem. Eng.
https://doi.org/10.1016/j.jece.2019.103212

[19] L. Atzori, M.G. Cutrufello, D. Meloni, R. Monaci, C. Cannas, D. Gazzoli, M.F. Sini, P. Deiana, E. Rombi (2017) CO_2 methanation on hard-templated NiO-CeO_2 mixed oxides. Int. J. Hydrog. Energ.
https://doi.org/10.1016/j.ijhydene.2017.06.198

[20] T.A. Le, M.S. Kim, S.H. Lee, T.W. Kim, E.D. Park (2017) CO and CO_2 methanation over supported Ni catalysts. Catal. Today.
https://doi.org/10.1016/j.cattod.2016.12.036

[21] A. Sápi, T. Rajkumar, M. Ábel, A. Efremova, A. Grósz, A. Gyuris, K.B. Ábrahámné, I. Szenti, J. Kiss, T. Varga, Á. Kukovecz, Z. Kónya (2019) Noble-metal-free and Pt nanoparticles-loaded, mesoporous oxides as efficient catalysts for CO_2 hydrogenation and dry reforming with methane. J. CO2 Util.
https://doi.org/10.1016/j.jcou.2019.04.004

[22] P. Tamizhdurai, S. Sakthinathan, S.-M. Chen, K. Shanthi, S. Sivasanker, P. Sangeetha (2017) Environmentally friendly synthesis of CeO_2 nanoparticles for the catalytic oxidation of benzyl alcohol to benzaldehyde and selective detection of nitrite. Sci Rep.
https://doi.org/10.1038/srep46372

[23] X. Dai, W. Jiang, W. Wanglong, X. Weng, Y. Shang, Y. Xue, Z. Wu (2018) upercritical water syntheses of transition metal-doped CeO_2 nano-catalysts for selective catalytic reduction of NO by CO: An in situ diffuse reflectance Fourier transform infrared spectroscopy study. Cheniese J. Catal.
https://doi.org/10.1016/S1872-2067(17)63008-0

[24] K.S.W. Sing (1986) Reporting physisorption data for gas/solid systems with special reference to the determination of surface area and porosity (Recommendations 1984). Pure & App!. Chem.
https://doi.org/10.1351/pac198557040603

[25] X. Wang, D. Liu, J. Li, J. Zhen, H. Zhang (2015) Clean synthesis of Cu_2O@CeO_2 core@shell nanocubes with highly active interface. NPG Asia Mater.
https://doi.org/10.1038/am.2014.128

[26] H. Yen, Y. Seo, S. Kaliaguine, F. Kleitz (2012) Tailored Mesostructured Copper/Ceria Catalysts with Enhanced Performance for Preferential Oxidation of CO at Low Temperature. Angew Chemie Int. Ed
https://doi.org/10.1002/anie.201206505

[27] X. Pang, Y. Chen, R. Dai, P. Cui (2012) Co/CeO_2 Catalysts Prepared Using Citric Acid Complexing for Ethanol Steam Reforming. Cheniese J. Catal.
https://doi.org/10.1016/S1872-2067(11)60335-5

[28] X. Zhang, R. You, D. Li, T. Cao, W. Huang (2017) Reaction Sensitivity of Ceria Morphology Effect on Ni/CeO_2 Catalysis in Propane Oxidation Reactions. ACS Appl. Mater. Interfaces.
https://doi.org/10.1021/acsami.7b11536

[29] J. Janlamool, P. Praserthdam, B. Jongsomjit (2011) Ti-Si composite oxide-supported cobalt catalysts for CO_2 hydrogenation. J. Nat. Gas Chem.
https://doi.org/10.1016/S1003-9953(10)60213-7

[30] O. Grad, M. Mihet, G. Blanita, M. Dan, L. Barbu-Tudoran, M.D. Lazar (2020) MIL-101-Al_2O_3 as catalytic support in the methanation of CO_2 – Comparative study between Ni/MIL-101 and Ni/MIL-101-Al_2O_3 catalysts. C. Catal. Today.
ttps://doi.org/10.1016/j.cattod.2020.05.003

[31] G. Zhou, T. Wu, H. Xie, X. Zheng (2013) Effects of structure on the carbon dioxide methanation performance of Co-based catalysts. Int. J. Hydrog. Energ.
https://doi.org/10.1016/j.ijhydene.2013.05.130

[32] L. Pastor-Pérez, M. Shah, E. Le Saché, T. Ramirez Reina (2018) Improving Fe/Al_2O_3 Catalysts for the Reverse Water-Gas Shift Reaction: On the Effect of Cs as Activity/Selectivity Promoter. Catalysts.
https://doi.org/10.3390/catal8120608

[33] J. Liu, C. Li, F. Wang, S. He, H. Chen, Y. Zhao, M. Wei, D.G. Evans, X. Duan (2013) Enhanced low-temperature activity of CO_2 methanation over highly-dispersed Ni/TiO_2 catalyst. Catal. Sci. Technol.
https://doi.org/10.1039/C3CY00355H

[34] J. Sun, Y. Wang, H. Zou, X. Guo, Z.-j. Wang (2019) Ni catalysts supported on nanosheet and nanoplate γ-Al_2O_3 for carbon dioxide methanation. J. Energy Chem.
https://doi.org/10.1016/j.jechem.2017.09.029

[35] G. Zhou, B. Dai, H. Xie, G. Zhang, K. Xiong, X. Zheng (2017) CeCu composite catalyst for CO synthesis by reverse water–gas shift reaction: Effect of Ce/Cu mole ratio. J. CO2 Util.

https://doi.org/10.1016/j.jcou.2017.07.004